Chapter 1
Passivity-Based Control Design and Experiments for a Rolling-Balancing System

Alejandro Donaire, Martin Crespo, Fabio Ruggiero, Vincenzo Lippiello and Bruno Siciliano

Key words: Rolling-ballancing System, Nonlinear Control, Passivity-based Control, Integral Action.

Abstract In this chapter we present the design and implementation of a robust passivity-based controller for a rolling-balancing system know as the disk-on-disk. The control design aims to asymptotically stabilize the desired equilibrium of the disk-on-disk by shaping the energy function of the system and injecting damping. This first design is further augmented by the addition of a nonlinear PID controller to compensate for disturbances. We incorporate in the nonlinear PID the possibility of stabilizing either a set-point of angular positions of the disks or their angular velocities while keeping the balance of the system. Although the underactuation feature of the system and the disturbances hampers the control design, we show that the passivity-based framework offers the necessary tools to prove the desired stability properties of the close loop. Finally, we evaluate the practical applicability of the control design by implementing the controller on a real hardware for the disk-on-disk system and asses the performance of the control system.

Alejandro Donaire, Fabio Ruggiero, Vincenzo Lippiello and Bruno Siciliano
PRISMA Lab, Dipartimento di Ingegneria Elettrica e Tecnologie dell'Informazione, Università di Napoli Federico II, Via Claudio 21, 80125 Napoli, Italy, e-mail: {alejandro.donaire,fabio.ruggiero,vincenzo.lippiello,bruno.siciliano}@unina.it

Martin Crespo
Departamento de Control, FCEIA, Universidad Nacional de Rosario and CONICET, Riobamba 245 bis, S2000EKE, Rosario, Argentina, e-mail: crespom@fceia.unr.edu.ar

1.1 INTRODUCTION

Control theory has provided a rich variety of methods for control design of nonlinear systems [5, 6]. In the context of robotics and mechanical systems, nonlinear methods have been widely used for control design (see e.g. [17, 18]). A class of mechanical systems posing a particularly challenging control problem is that of underactuated mechanical systems. Underactuation refers to the fact that number of the inputs is smaller than the number of the degrees of freedom.

Passivity-based control (PBC) has shown to be a successful technique for control design of underactuated systems [11]. A standard constructive method for stabilization of mechanical system is the so-called interconnection and damping assignment (IDA) [12]. This technique is based on Lagrange-Dirichlet result on stability of mechanical systems, which states that an isolated minimum of the potential energy is Lyapunov stable (see Theorem 3.1 in [9] for further details). The basic idea of IDA-PBC is to shape the energy of the system and assign a minimum at the desired equilibrium by using feedback measurements and the control input. A further injection of damping is needed to ensure asymptotic stability [13]. To stabilize a desired equilibrium for fully actuated systems, only the potential energy of the system is needed to be shaped. However, both the potential and kinetic energies have to be shaped to stabilize underactuated systems, a procedure known as total energy shaping. Although passivity-based controllers are known to be robust against parameter uncertainties, the action of external disturbances can deteriorate the performance of the closed loop or, even worse, produce instabilities. To address this problem, a classical addition of control actions has been proposed in [2, 10]. This integral action design has been specialised for fully actuated and underactuated mechanical system by [14] and [3], respectively.

In this work, we consider the control problem of the disk-on-disk (DoD), which is an underactuted rolling-balancing system [16]. The DoD is a case study of *non-prehensile manipulation* and has been used as testbed for control designs in this context [4, 16]. In addition to the stabilization problems of angular position set-points or tracking constant angular speed while keeping balance, we also consider input disturbances, which complicate the design. Previous works have considered the stabilization problem of the DoD using exact-feedback linearization [8], and energy shaping [4], but none of these works consider disturbances in the design. The work in [15] considers constant speed tracking but disturbances were no considered. In our work, we explicitly consider the disturbances and we design a robust IDA-PBC controller following the approach proposed by [3]. This controller results in a classical IDA-PBC inner controller plus a nonlinear PID-type outer-loop controller, which rejects the disturbance. In addition, we implement the control laws in a real hardware for the disk-on-disk prototype, and run a set of experiments. These experiments allow assessing the performance of the controllers and evaluating the practical applicability of the methods provided in the literature of control theory.

The rest of the chapter is organized as follows: Section 1.2 reviews the basic background on port-Hamiltonian framework and IDA-PBC. The control design for the disk-on-disk is developed in Section 1.3. Section 1.4 presents simulations and

experiment results, respectively. Finally, the chapter is wrapped-up with the conclusions.

Caveat. This chapter is an extended version of the conference paper presented at ICINCO 2016 [1].

1.2 PORT-HAMILTONIAN SYSTEMS

1.2.1 Hamiltonian Models

A broad class of mechanical systems can be described by the Euler-Lagrange equations of motion

$$\frac{d}{dt}\left[\nabla_{\dot{q}}\mathscr{L}(q,\dot{q})\right]-\nabla_{q}\mathscr{L}(q,\dot{q})=G(q)u, \tag{1.1}$$

where $q\in\mathbb{R}^n$ is the generalized position, u the input force, $G:\mathbb{R}^n\to\mathbb{R}^{n\times m}$ is the input matrix and $\mathscr{L}$ the Lagrangian, which as the following form

$$\mathscr{L}(q,\dot{q})=\frac{1}{2}\dot{q}^{\top}M(q)\dot{q}-V(q),$$

where $V:\mathbb{R}^n\to\mathbb{R}$ is the potential energy and $M:\mathbb{R}^n\to\mathbb{R}^{n\times n}$ is the mass matrix and satisfies the condition $M(q)=M^{\top}(q)>0$. Applying the Legendre transformation and defining the generalized momentum $p=M(q)\dot{q}$ [7], we can express the dynamics (1.1) in the Hamiltonian form as follows

$$\begin{bmatrix}\dot{q}\\ \dot{p}\end{bmatrix}=\begin{bmatrix}0_{n\times n} & I_n\\ -I_n & 0_{n\times n}\end{bmatrix}\begin{bmatrix}\nabla_q H\\ \nabla_p H\end{bmatrix}+\begin{bmatrix}0_{n\times m}\\ G(q)\end{bmatrix}u \tag{1.2}$$

where $p\in\mathbb{R}^n$ and $H:\mathbb{R}^{n\times n}\to\mathbb{R}$ is the total energy system given as

$$H(q,p)=\frac{1}{2}p^{\top}M^{-1}(q)p+V(q). \tag{1.3}$$

1.2.2 Energy Shaping and Damping Assignment

The stabilization problem of the system (1.2) using IDA-PBC is to find a control input u such that the dynamics of the closed loop can be written as a port-Hamiltonian system as follows

$$\begin{bmatrix}\dot{q}\\ \dot{p}\end{bmatrix}=\begin{bmatrix}0_{n\times n} & M^{-1}M_d\\ -M_dM^{-1} & J_2-R_d^{\top}\end{bmatrix}\begin{bmatrix}\nabla_q H_d\\ \nabla_p H_d\end{bmatrix} \tag{1.4}$$

where the matrices $J_2(q,p) = J_2^\top(q,p)$ and $R_d(q) = G^\top(q)K_vG(q)$ represent the desired interconnection and damping structures, respectively, and $K_v > 0$ is a free symmetric matrix to be chosen. The function $H_d : \mathbb{R}^n \to \mathbb{R}$ is the desired energy in closed loop which has the form

$$H_d(q,p) = \frac{1}{2}p^\top M_d^{-1}(q)p + V_d(q) \tag{1.5}$$

where $M_d(q) = M_d^\top(q) > 0$ and $V_d(q)$ are the desired mass matrix and the desired potential energy of the closed loop, respectively. In addition, if $q^\star$ is a minimum of the potential energy, then the desired energy H_d qualifies as a Lyapunov candidate function, and its time derivative along the solutions of (1.4) results as follows

$$\dot{H}_d = -p^\top M_d^{-1}G^\top K_vGM_d^{-1}p \leq 0, \tag{1.6}$$

which ensures that $q^\star$ is a stable equilibrium of the closed-loop system. Moreover, asymptotic stability follows if the signal $y_d = GM_d^{-1}p$ is detectable [12].

The classical approach to design an IDA-PBC controller is to compute the control in two steps. First, the energy shaping control $u_{\mathtt{ES}}$, and second the damping injection $u_{\mathtt{DI}}$. Then, the control input is obtained as $u = u_{\mathtt{ES}} + u_{\mathtt{DI}}$. The energy shaping controller is computed by matching the open dynamics (1.2) and the desired closed loop (1.4) assuming $R_d = 0$. This procedure results in the following matching equation

$$\begin{bmatrix} 0_{n\times n} & I_n \\ -I_n & 0_{n\times n} \end{bmatrix}\begin{bmatrix} \nabla_q H \\ \nabla_p H \end{bmatrix} + \begin{bmatrix} 0_{n\times m} \\ G(q) \end{bmatrix} u_{\mathtt{es}} = \begin{bmatrix} 0_{n\times n} & M^{-1}M_d \\ -M_dM^{-1} & J_2 \end{bmatrix}\begin{bmatrix} \nabla_q H_d \\ \nabla_p H_d \end{bmatrix}, \tag{1.7}$$

which should be solve for $u_{\mathtt{ES}}$. For the nontrivial case of underactuated systems, where $G(q)$ is full column rank but non invertible matrix, the solution of (1.7) can be found by solving the following two equations:

- Kinetic-energy matching equation (KE-ME)

$$G^\perp\Big\{\nabla_q\Big[p^\top M^{-1}p\Big] - M_dM^{-1}\nabla_q\Big[p^\top M_d^{-1}p\Big] + 2J_2M_d^{-1}p\Big\} = 0 \tag{1.8}$$

- Potential-energy matching equation (PE-ME)

$$G^\perp\Big\{\nabla_q V - M_dM^{-1}\nabla_q V_d\Big\} = 0, \tag{1.9}$$

where $G^\perp \in \mathbb{R}^{(n-m)\times n}$ is the full rank left annihilator of G, i.e. $G^\perp G = 0$. Then, the energy shaping control law is given by

$$u_{\mathtt{ES}} = (G^\top G)^{-1}G^\top\Big[\nabla_q H - M_dM^{-1}\nabla_q H_d + J_2\nabla_p H_d\Big]. \tag{1.10}$$

The second step in the design is the damping injection, which is given by the control law

$$u_{\mathtt{DI}} = -K_vG^\top M_d^{-1}p. \tag{1.11}$$

As discussed by [12], the injection of damping together with the detectability condition are needed for asymptotic stability.

1.3 CONTROL DESIGN FOR THE DISK-ON-DISK

1.3.1 Dynamic Model

The DoD is a rolling-balancing system shown in Figure 1.1. Disk 1 is actuated by a controlled torque whilst Disk 2 is non-actuated (see [16] for a detailed modelling development). We consider two control objectives:

O.1 Stabilization of the Disk 2 at the upright position while driving the angle of Disk 1 to a target angular reference.

O.2 Tracking of constant angular velocities reference for Disk 1 while keeping the Disk 2 at the upright position.

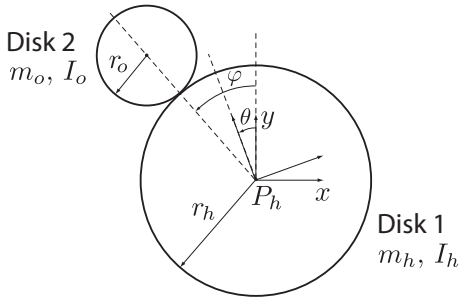

Fig. 1.1 A schematic of the DoD system.

The dynamic model of the DoD can be described by the Lagrangian equations in coordinates (θ, φ), where θ is the angle of Disk 1, and φ is the deviation angle of Disk 2 respect to the upright position. The Langrangian for the DoD is given by

$$\mathscr{L}(q,\dot{q}) = \frac{1}{2}\begin{bmatrix}\dot{\theta} & \dot{\varphi}\end{bmatrix}^{\top}\begin{bmatrix}M_{11} & M_{12}\\ M_{21} & M_{22}\end{bmatrix}\begin{bmatrix}\dot{\theta} & \dot{\varphi}\end{bmatrix} - V(q) \tag{1.12}$$

where

$$V(q) = V_0\cos(\varphi)$$

with $V_0 = m_o g(r_o + r_h)$. The function V represents the potential energy and M is the mass matrix whose entries are

$$\begin{aligned} M_{11} &= r_h^2(m_o + m_h)\\ M_{12} &= M_{21} = -m_o r_h(r_o + r_h)\\ M_{22} &= 2m_o(r_o + r_h)^2 \end{aligned}$$

Equivalently, as explained in Section 1.2, the DoD model can be written in the Hamiltonian form as follows

$$\begin{bmatrix}\dot{q}\\ \dot{p}\end{bmatrix} = \begin{bmatrix}0 & I\\ -I & 0\end{bmatrix}\begin{bmatrix}\nabla_q H\\ \nabla_p H\end{bmatrix} + \begin{bmatrix}0\\ G\end{bmatrix} u \tag{1.13}$$

where the coordinates $q = \begin{bmatrix}\theta & \varphi\end{bmatrix}^\top$, the momenta $p = M\dot{q}$ and the input matrix $G = \begin{bmatrix}1 & 0\end{bmatrix}^\top$. The Hamiltonian function is

$$H(q,p) = \frac{1}{2}p^\top M^{-1} p + V(q).$$

1.3.2 Energy Shaping and Damping Assignment Control

The objective in this section is to design a IDA-PBC controller for the DoD system that stabilises the point $q^* = (\theta^*, 0)$, where θ^* is the desired equilibrium for Disk 1 angle. This control objective corresponde to the task **O.1** describe in section 1.3.1. To solve this problem we design a controller using energy shaping and damping injection as described in Section 1.2. That is, we search for the function V_d and the matrices M_d and J_2 that solve the KE-ME and PE-ME, (1.8) and (1.9) respectively. Thus, the energy shaping control is obtained from (1.10) and the damping injection control from (1.11).

Since the mass matrix of the DoD is constant and does not depend on the coordinates q, we select M_d as a constant matrix as follows

$$M_d = \begin{bmatrix}N_{11} & N_{12}\\ N_{12} & N_{22}\end{bmatrix}$$

where N_{11}, N_{12} and N_{22} are free constants parameters. To simplify the notation, we note

$$M_d M^{-1} = \begin{bmatrix}a & b\\ c & d\end{bmatrix}.$$

Then, the PE-ME (1.9) is as follows

$$\begin{aligned}\begin{bmatrix}0 & 1\end{bmatrix}\left\{\begin{bmatrix}0\\ V_0\sin(\varphi)\end{bmatrix} + \begin{bmatrix}a & b\\ c & d\end{bmatrix}\begin{bmatrix}\nabla_\theta V_d\\ \nabla_\varphi V_d\end{bmatrix}\right\} &= 0\\ V_0\sin(\varphi) + c\,\nabla_\theta V_d + d\,\nabla_\varphi V_d &= 0.\end{aligned} \tag{1.14}$$

We solve the partial differential equation (1.14) for V_d, and we obtain, using a symbolic software (e.g. Mathematica, Maple), a solution as follows

$$V_d(q) = \frac{1}{d}V_0\cos(\varphi) + \frac{k_2}{2}\left(\theta - \frac{c}{d}\varphi - k_1\right)^2 \tag{1.15}$$

where k_1 and k_2 are free constant parameters to be chosen to assign a minimum at the desired equilibrium.

From the previous selection of M_d, it is clear that the KE-ME (1.8) is satisfied by choosing $J_2(q,p)=0$. In addition, we need to ensure that $M_d>0$ and that V_d has an isolated minimum at the desired equilibrium $q^\star$.

The minimum of V_d is assigned by requiring that the Jaccobian and Hessian evaluated at $q^\star$ are zero and positive definite respectively. Then, we compute

I) $\nabla_q V_d(q)\big|_{q=q^*}=0 \Leftrightarrow \left[\begin{array}{c} k_2\left(\theta-\frac{c}{d}\varphi-k_1\right) \\ \frac{-V_0}{d}\sin(\varphi)-\frac{k_2 c}{d}\left(\theta-\frac{c}{d}\varphi-k_1\right)\end{array}\right]\Bigg|_{q=q^*}=0$

which is satisfied if $k_1=\theta^*$.

II) $\nabla_q^2 V_d(q)\big|_{q=q^*}>0 \Leftrightarrow \left[\begin{array}{cc} k_2 & -k_2\frac{c}{d} \\ -k_2\frac{c}{d} & \frac{-V_0}{d}\cos(\varphi)+k_2\left(\frac{c}{d}\right)^2\end{array}\right]\Bigg|_{q=q^*}>0$

which is satisfied provided that $k_2>0$ and $d<0$ (equivalently $N_{12}M_{12}-N_{22}M_{11}>0$).

The positive definiteness of M_d is ensured if $N_{11}>0$ and $N_{11}N_{22}-N_{12}^2>0$.

Notice that effectively, the potential energy has a minimum at the desired equilibrium $(\theta^\star,\varphi^\star)=(0,0)$ as shown in Figure 1.2, where we have used the values of the parameters as in Section 1.4.1 for illustrative purpose.

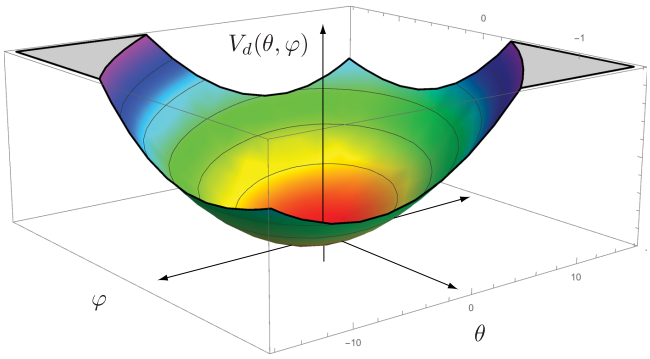

Fig. 1.2 Desired potential energy.

Finally, the control law is computed from (1.10) and (1.11) as follows

$$u=u_{\mathtt{es}}+u_{\mathtt{DI}}=-\frac{b}{d}\nabla_\varphi V-k_2\left(\frac{ad-bc}{d}\right)\left(\theta-\frac{c}{d}\varphi-\theta^\star\right)-K_v\,d\,\sigma\left(\dot\theta-\frac{c}{d}\dot\varphi\right) \tag{1.16}$$

where $\sigma=\frac{M_{11}M_{22}-M_{12}^2}{N_{11}N_{22}-N_{12}^2}$ and the free parameters N_{11}, N_{12}, N_{22}, k_2 and K_v should satisfy

$$N_{11} > 0, \quad k_2 > 0, \quad K_v > 0,$$
$$N_{11}N_{22} - N_{12}^2 > 0,$$
$$N_{12}M_{12} - N_{22}M_{11} > 0.$$

Thus, the dynamics of the DoD system (1.13) in closed loop with the controller (1.16) can be written in the Hamiltonian form

$$\begin{bmatrix} \dot{q} \\ \dot{p} \end{bmatrix} = \begin{bmatrix} 0 & M^{-1}M_d \\ -M_dM^{-1} & -GK_vG^\top \end{bmatrix} \begin{bmatrix} \nabla_q H_d \\ \nabla_p H_d \end{bmatrix} \tag{1.17}$$

To analyse the stability of the closed loop (1.17), we consider the desired Hamiltonian in (1.5) as a Lyapunov function and we compute its time derivative as follows

$$\begin{aligned} \dot{H}_d(q,p) &= p^\top M_d^{-1}\dot{p} + \dot{q}^\top \dot{V}_d(q) \\ &= p^\top M_d^{-1}\left(-M_dM^{-1}\dot{V}_d - GK_vG^\top M_d^{-1}p\right) + \dot{q}^\top \dot{V}_d(q) \\ &= -p^\top M_d^{-1}GK_vG^\top M_d^{-1}p \leq 0, \end{aligned}$$

which ensures stability of the desired equilibrium. Asymptotic stability follows from LaSalle's invariance principle [6], or equivalently from detectability of the signal $y_d = K_vG^\top M_d^{-1}p$ [19].

1.3.3 Effect of Input Disturbances

Now, we consider the presence of a matched disturbance δ in the closed loop (1.17). In this case, the closed-loop dynamics is

$$\begin{bmatrix} \dot{q} \\ \dot{p} \end{bmatrix} = \begin{bmatrix} 0 & M^{-1}M_d \\ -M_dM^{-1} & -GK_vG^\top \end{bmatrix} \begin{bmatrix} \nabla_q H_d \\ \nabla_p H_d \end{bmatrix} + \begin{bmatrix} 0 \\ G \end{bmatrix} (v + \delta) \tag{1.18}$$

where δ is the matched constant disturbance and v is a control input that will be used to reject the unknown disturbance. To obtain the dynamics (1.18), we use the control $u = u_{\texttt{es}} + u_{\texttt{DI}} + v$ in (1.13), and we add the disturbance. Notice that the disturbance shifts the equilibrium of the closed loop, defined by zero velocities (equivalently $p = 0$), from the desired equilibrium $q^\star$ to a new equilibrium $\bar{q}$, which is the solution of

$$-M_dM^{-1}\nabla_q V_d + G\delta = 0,$$

which implies that $\bar{q} = (\bar{\theta}, \bar{\varphi})$ with $\bar{\theta} = \theta^\star + \frac{d}{(ad-bc)k_2}\delta$ and $\bar{\varphi} = 0$. This shows that the control objective is not achieved by the controller in the presence of constant disturbances, since θ will not reach the desired value at steady state as desired. This motivates us to implement outer-loop controllers to reject constant unknown disturbances.

1.3.4 Robust Energy Shaping

In this section, we implement three integral based controllers proposed in [3] to enhance the robustness of energy shaping controller. We develop these integral controllers for the disk-on-disk in closed loop with the control (1.16). That is, for the closed-loop dynamics (1.17) we design a control law v to reject constant disturbances δ. We first present the most complex controller which is a nonlinear PID, and subsequently we present two simpler versions, which result in a type of PI and PID controllers. We also extend this control design to ensure the second control objective **O.2**, which is to ensure tracking of constant angular velocities.

1.3.4.1 Integral control

The fundamental idea proposed by [3] is to find a dynamic control law $v(q,p,\zeta)$, where ζ is the state of the controller, and a change of coordinates such that the closed loop in the new coordinates can be written as a Hamiltonian system, thus stability is ensured. For the DoD closed loop (1.18), we proposed a target Hamiltonian system in new coordinates $z \in \mathbb{R}^5$, where we have augmented the state vector by adding the controller state. The target Hamiltonian system is

$$\begin{bmatrix} \dot{z_1} \\ \dot{z_2} \\ \dot{z_3} \end{bmatrix} = \begin{bmatrix} -\Gamma_1 & M^{-1}M_d & -\Gamma_2 \\ -M_dM^{-1} & -GK_vG^\top & -GK_3 \\ \Gamma_2^T & K_3^TG^T & -\Gamma_3 \end{bmatrix} \begin{bmatrix} \nabla_{z_1}H_z \\ \nabla_{z_2}H_z \\ \nabla_{z_3}H_z \end{bmatrix} \tag{1.19}$$

with Hamiltonian

$$H_z(z) = \frac{1}{2}z_2^\top M_d^{-1}z_2 + V_z(z_1) + \frac{1}{2}K_I(z_3 - z_3^\star)^2 \tag{1.20}$$

where

$$V_z(z_1) = V_d(q)\Big|_{q=z_1} = \frac{1}{d}V_0\cos(z_{12}) + \frac{k_2}{2}\left(z_{11} - \frac{c}{d}z_{12} - k_1\right)^2, \tag{1.21}$$

with $z_1 = \begin{bmatrix} z_{11} & z_{12} \end{bmatrix}^\top$ and constant gains equal to

$$\begin{aligned} \Gamma_1 &\triangleq M^{-1}GK_1G^TM^{-1} \\ \Gamma_2 &\triangleq M^{-1}GK_2 \\ \Gamma_3 &\triangleq K_3^TG^TM_d^{-1}GK_2 \\ z_3^\star &\triangleq \frac{\delta}{K_I\left(K_vG^TM_d^{-1}GK_2 + K_3\right)} \end{aligned}$$

where the new coordinates $z = \psi(q,p,\zeta)$ are obtained by the state transformation

$$z_1 = q - G(\alpha t + \beta) \tag{1.22}$$
$$z_2 = p + GK_1G^TM^{-1}\nabla V_z + GK_2K_I(\zeta - z_3^\star) - MG\alpha \tag{1.23}$$
$$z_3 = \zeta \tag{1.24}$$

with $K_v > 0$, $K_I > 0$, $K_1 > 0$, $K_3 > 0$ and $K_2 = \left(G^\top M_d^{-1} G\right)^{-1}$. The values of α and β characterizes the ramp profile of the angle reference that should be tracked by the Disk 1. Notice that when z_1 converge to zero, then q converge to $G(\alpha t + \beta)$. Therefore, we look for a control law that render the closed-loop dynamics in the form (1.19), and we study the stability properties of such system at the origin. To obtain such control law, we first notice that if we differentiate (1.22) and replace the derivative of the states by their corresponding state equations from (1.18) and (1.19), we obtain

$$\begin{aligned}
\dot{z}_1 &= \dot{q} - G\alpha \\
&= M^{-1}p - G\alpha \\
&= M^{-1}\left[z_2 - GK_1G^TM^{-1}\nabla V_z - GK_2K_I(\zeta - z_3^\star) + MG\alpha\right] - G\alpha \\
&= -\Gamma_1\nabla_{z_1}H_z + M^{-1}M_d\nabla_{z_2}H_z - \Gamma_2\nabla_{z_3}H_z,
\end{aligned} \tag{1.25}$$

which implies that the dynamics of z_1 expressed in the new coordinates z is exactly the first row of (1.19).

Similarly, to construct the dynamics of z_2 as in the second row of (1.19), we differentiate (1.23) as follows

$$\begin{aligned}
\dot{z}_2 &= \dot{p} + GK_1G^TM^{-1}\nabla^2 V_z\dot{z}_1 + GK_2K_I\dot{z}_3 \\
&= -M_dM^{-1}\nabla V_d - GK_vG^\top M_d^{-1}p + Gv + G\delta + GK_1G^TM^{-1}\nabla^2 V_z(\dot{q} - G\alpha) + \\
&\quad GK_2K_I\dot{z}_3.
\end{aligned} \tag{1.26}$$

from where we can see that to obtain the desired dynamics for z_2, the control law should satisfy

$$\begin{aligned}
Gv = \dot{z}_2 + M_dM^{-1}\nabla V_d + GK_vG^\top M_d^{-1}p - G\delta - GK_1G^TM^{-1}\nabla^2 V_z(\dot{q} - G\alpha) - \\
GK_2K_I\dot{z}_3.
\end{aligned} \tag{1.27}$$

Replacing $\dot{z}_2$ and $\dot{z}_3$ in (1.27) for the second and third row of (1.19), respectively, and noticing that $G^\perp[M_dM^{-1}\nabla V_z - M_dM^{-1}\nabla V_d] = 0$, then the control law as a function of (q, p, ζ) results, after some calculations, as follows

$$v = -\left[K_v G^\top M_d^{-1} G K_1 G^\top M^{-1} + K_2 K_I \left(K_2^\top + K_3^\top G^\top M_d^{-1} G K_1\right) G^\top M^{-1}\right] \nabla V_d -$$
$$\left[K_1 G^\top M^{-1} \nabla^2 V_d M^{-1} + K_2 K_I K_3^\top G^\top M_d^{-1}\right] p - \left(K_v G^\top M_d^{-1} G K_2 + K_3\right) K_I \zeta +$$
$$\left[K_v G^\top M_d^{-1} + K_1 G^\top M^{-1} \nabla^2 V_d M^{-1} + K_2 K_I K_3^\top G^\top M_d^{-1}\right] MG\alpha -$$
$$(G^\top G)^{-1} G^\top M_d M^{-1} \left[\nabla V_z - \nabla V_d\right]. \tag{1.28}$$

Finally, the dynamics of z_3, or equivalently ζ, can be freely set as in the third row of (1.19), which can be written as follows

$$\dot{\zeta} = \left(K_2^\top + K_3^\top G^\top M_d^{-1} G K_1\right) G^\top M^{-1} \nabla V_d + K_3^\top G^\top M_d^{-1} p -$$
$$K_3^\top G^\top M_d^{-1} MG\alpha. \tag{1.29}$$

The controller, compose by the control law (1.28) and the integrator (1.29), does not required the information of the constant disturbance δ.

We have shown that the dynamics (1.18) in closed loop with the nonlinear PID controller (1.28)-(1.29) can be written in the form (1.19). The Hamiltonian form of the closed-loop dynamics ensures its stability. Indeed, the Hamiltonian in (1.20) has a minimum at the desired equilibrium $(z_1, z_2, z_3) = (0, 0, z_3^\star)$ if $k_1 = 0$, and it qualifies as a Lyapunov function for the dynamics (1.19). The time derivative of H_z is

$$\dot{H}_z = -\nabla^\top V_d(z_1) M^{-1} G K_1 G^\top M^{-1} \nabla V_z - z_2^\top M_d^{-1} G K_v G^\top M_d^{-1} z_2 - \Gamma_3 K_I^2 (z_3 - z_3^\star)^2$$
$$\leq 0,$$

which ensures stability. Asymptotic stability follows using LaSalle argument and noticing that the maximum invariant set included in $\mathscr{S} = \{(z_1, z_2, z_3) | G^\top M^{-1} \nabla V_z = 0, G^\top M_d^{-1} z_2 = 0, z_3 = z_3^\star\}$ is the desired equilibrium $(0, 0, z_3^\star)$.

Notice that the controller (1.28) is a nonlinear PID, which we will refer as NLPID2. Moreover, two simpler version of this controller can be obtained by setting the controller parameters to particular values. Indeed, a simpler nonlinear PID can be considering $K_2 = 0$ and $K_3 = 1$, which we will refer to as NLPID1, and a nonlinear PI controller is obtained by setting $K_1 = 0$ and $K_3 = 0$, which will refer to as NLPI.

In addition, we point out that a controller with only the integral of the passive outputs, which are the velocities form mechanical systems, can be obtained by setting $K_1 = 0$, $K_2 = 0$ and $K_3 = K_I^{-1}$. We will refer to this controller as IA. It has been shown in [14] that this type of integral action does not reject disturbances, destroys the detectability of the passive outputs and creates a manifold of equilibrium. Thus asymptotic stability is not achieved, a fact that is seen in the experiments.

1.4 SIMULATIONS AND EXPERIMENTS

In this section we present simulation and experiment results to assess the performance of the controllers presented in Section 1.3 and verify their applicability in a real setup. The simulations are performed using Matlab and the experiments are carried out the prototype show in Figure 1.3 available at PRISMA Lab. The model parameters of the disk-on-disk are $m_h = 0.335$ Kg, $m_o = 0.22$ Kg, $r_h = 0.15$ m and $r_o = 0.075$ m.

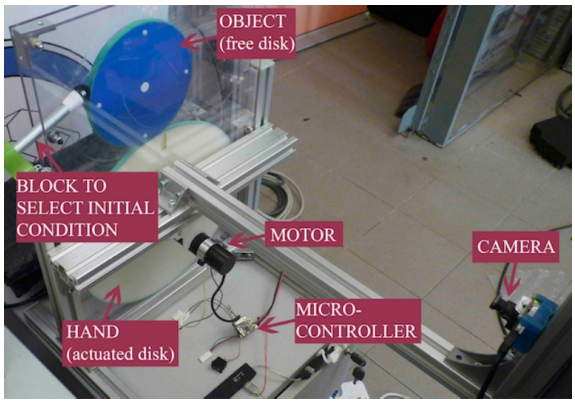

Fig. 1.3 Prototype of the disk-on-disk available at PRISMA Lab.

The prototype consists of two disks placed in between two plastic panels. Disk 1 is actuated by a DC motor (Harmonic Drive RH–8D 3006) equipped with a harmonic drive whose gearhead ratio is 100 : 1, and a 500 p/r quadrature encoder. A rubber band of about 1 mm encircles both disks to avoid slipping. The commands to the motor are provided by an ARM CORTEX M3 microcontroller (32 bit, 75 MHz). This microcontroller receives current references from an external PC through a USB cable. The measurements of Disk 1 are provided by a encoder while the measurements of Disk 2 are provided by an external visual system. This consists of a uEye UI-122-xLE camera providing (376×240) pixel images to the PC at 75 Hz, that is also the controller sample rate. In order to speed up computations, a (15×15) pixel RoI is employed by the image elaboration algorithm running on the same external PC. The control algorithm, which is written in C++, runs on the external PC with a Linux-based operating system.

We have tested five different controllers in the prototype: i) the standar IDA-PBC controller, ii) the IDA-PBC controller augmented with the IA, iii) the IDA-PBC controller enhanced with the NLPID1, iv) the IDA-PBC controller enhanced with the NLPID2, and v) the IDA-PBC controller enhanced with the NLPI. The experiments are executed under the following scenarios: the initial conditions of the balancing and Disk 1 angles are $\varphi(0) = 7$ deg and $\theta(0) = 0$ deg respectively, whilst the angular velocities at starting time are zero. The set-point reference for the position of Disk 1 position is set to zero ($\theta^\star = 0$), while Disk 2 has to be stabilized at

the upright position. A constant matched disturbance of value $\delta = 0.01$ Nm is added to the system to evaluate the disturbance rejection properties of the controller.

1.4.1 Standard IDA-PBC

In the first experiment, we evaluate the performance of the IDA-PBC controller (1.16) stand alone. The parameters of the controller used in the experiment are $N_{11} = 0.41$, $N_{12} = -0.03$, $N_{22} = 0.003$, $k_2 = 0.0005$ and $K_v = 0.08$.

The results of this experiment are shown in Figures 1.4 to 1.6. As expected, the controller stabilizes Disk 2 at the upright position as shown in Figure 1.4. However, it is unable to ensure convergency of the angle of Disk 1 to the desired reference due to the disturbance (see Figure 1.5). The time history of the control torque is shown in Figure 1.6, which shows that the controller demands a reasonable torque without large sparks.

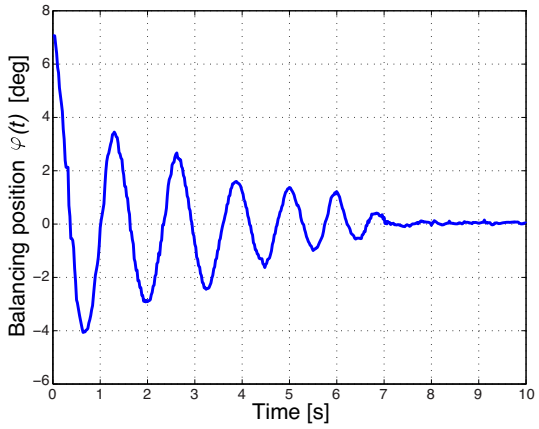

Fig. 1.4 Time history of the balancing angle with the IDA-PBC controller.

1.4.2 IDA-PBC plus IA

In the second experiment, we test the performance of the IDA-PBC controller plus the IA, that is the controller (1.16) plus (1.28) with $K_1 = 0$, $K_2 = 0$ and $K_3 = K_I^{-1}$. The parameters of the controller used in the experiment are $N_{11} = 0.41$, $N_{12} = -0.03$, $N_{22} = 0.003$, $k_2 = 0.0005$, $K_v = 0.08$, $\alpha = 0$, $\beta = 0$ and $K_I = 20$.

The results of this experiment are shown in Figures 1.7-1.10. Similar to the previous experiment, the controller balances Disk 2 at the upright position, but does not make the angle of Disk 1 converge to zero, which approaches a value of -160 degrees instead (see Figures 1.7 and 1.8). The state of the controller is shown in

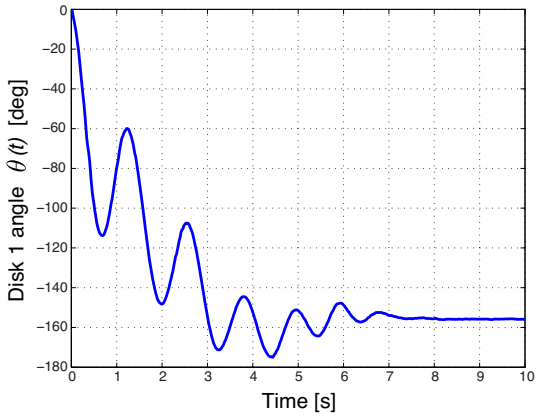

Fig. 1.5 Time history of Disk 1 angle with the IDA-PBC controller.

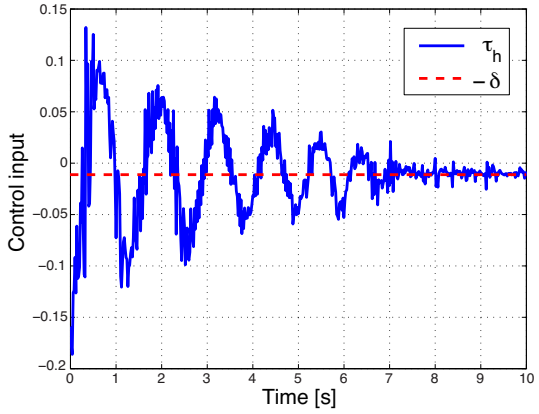

Fig. 1.6 Time history of the control input torque and its value at steady state with the IDA-PBC controller.

Figure 1.9, which reaches a value in the equilibrium manifold that has no relation with the disturbance. Finally, the control torque is plotted in Figure 1.10. This experiment illustrates that the integral action on the velocities does not produce any benefit when used to reject disturbances, as predicted by the theory.

1.4.3 IDA-PBC plus NLPI

In this fourth experiment, we evaluate the performance of the IDA-PBC controller plus the NLPI, that is the controller (1.16) plus (1.28) with $K_1 = 0$ and $K_3 = 0$. The parameters of the controller used in the experiment are $N_{11} = 0.41$, $N_{12} = -0.03$, $N_{22} = 0.003$, $k_2 = 0.0006$, $K_v = 1.5$, $K_2 = \left(G^\top M_d^{-1} G\right)^{-1}$ and $K_I = 1.6$.

The results of this experiment are shown in Figures 1.11-1.14. The plots in Figure 1.11 and 1.12 show that the controller stabilizes Disk 2 at the upright position and drives Disk 1 to the desired reference angle despite the action of the disturbance. However, a small error (less than one degree) on the angle φ can be seen in steady

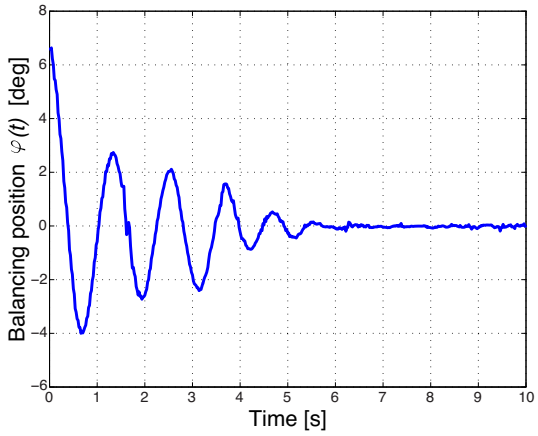

Fig. 1.7 Time history of the balancing angle with the IDA-PBC plus IA controller.

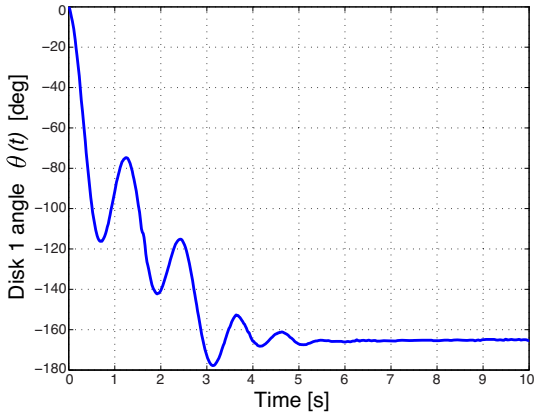

Fig. 1.8 Time history of Disk 1 angle with the IDA-PBC plus IA controller.

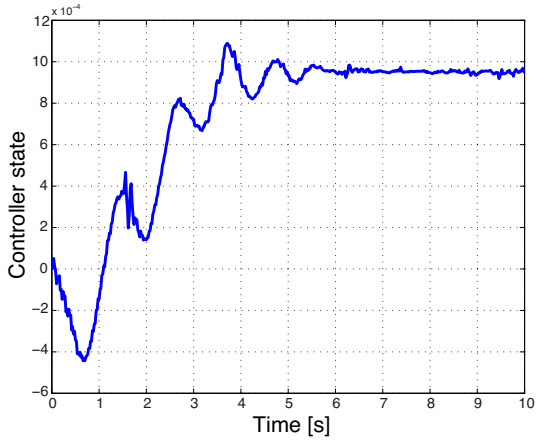

Fig. 1.9 Time history of the controller state and its value at steady state with the IDA-PBC plus IA controller.

state. Figure 1.13 shows that the state of the controller converges to the value needed

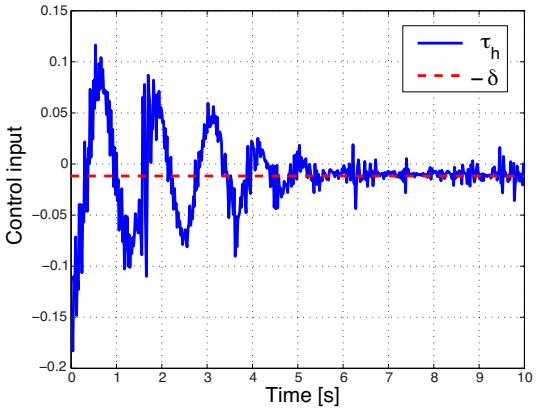

Fig. 1.10 Time history of the control input torque and its value at steady state with the IDA-PBC plus IA controller.

to compensate the disturbance, and Figure 1.14 depicts the control torque, which is bounded between admissible limits.

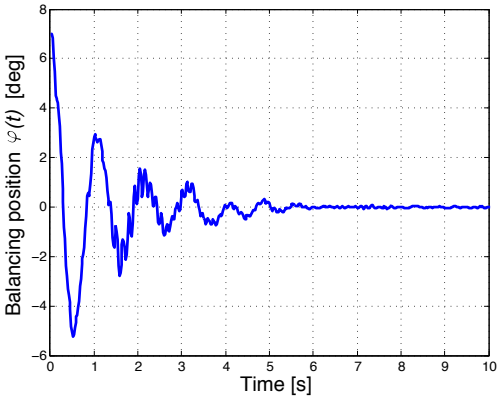

Fig. 1.11 Time history of the balancing angle with the IDA-PBC plus NLPI controller.

1.4.4 IDA-PBC plus NLPID1

In the second set of experiments, we evaluate the performance of the IDA-PBC controller plus the NLPID1, that is the controller (1.16) plus (1.28) with $K_2 = 0$ and $K_3 = 1$. The parameters of the controller are as follows: $N_{11} = 0.41$, $N_{12} = -0.03$, $N_{22} = 0.003$, $k_2 = 0.00048$, $K_1 = 0.00905$, $K_v = 0.35$, $\alpha = 0$, $\beta = 0$ and $K_I = 2.3$.

Figures 1.15 to 1.18 show the results of this experiment. The time history of the deviation angle of Disk 2 respect to the upright position is depicted in Figure 1.15. This figure shows that Disk 2 is balanced as desired. Figure 1.16 shows that the angle of Disk 1 reaches the reference value, and the controller rejects the disturbance.

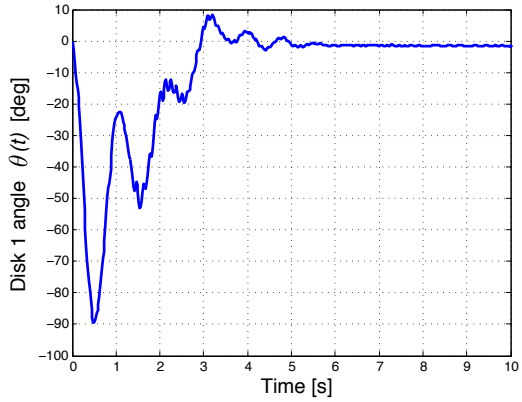

Fig. 1.12 Time history of Disk 1 angle with the IDA-PBC plus NLPI controller.

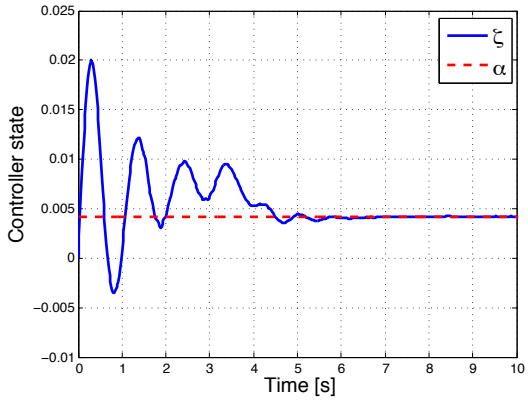

Fig. 1.13 Time history of the controller state and its value at steady state with the IDA-PBC plus NLPI controller.

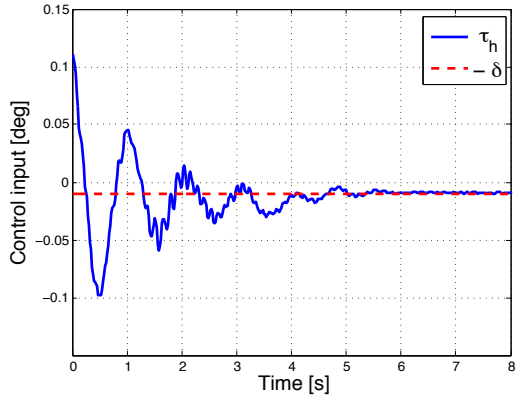

Fig. 1.14 Time history of the control input torque and its value at steady state with the IDA-PBC plus NLPI controller.

Also, it can be seen in Figure 1.17 that the controller state produces an estimate of the disturbance, which is used to compensate it. In addition, the control input is shown in Figure 1.18.

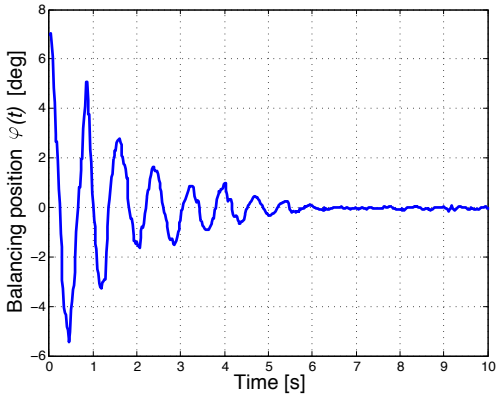

Fig. 1.15 Time history of the balancing angle with the IDA-PBC plus NLPID1 controller.

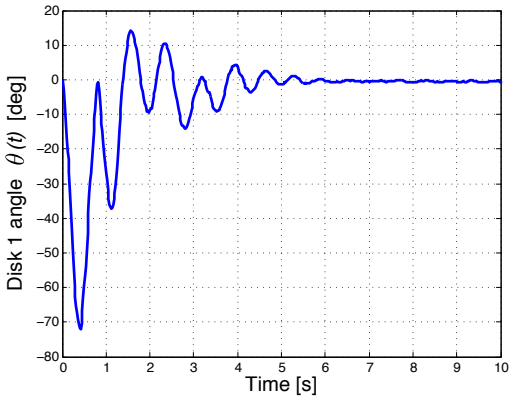

Fig. 1.16 Time history of Disk 1 angle with the IDA-PBC plus NLPID1 controller.

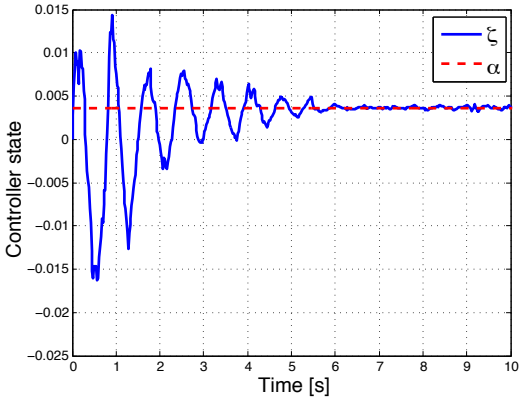

Fig. 1.17 Time history of the controller state and its value at steady state with the IDA-PBC plus NLPID1 controller.

1.4.5 IDA-PBC plus NLPID2

In the last experiment, we evaluate the performance of the IDA-PBC controller plus the NLPID2, that is the controller (1.16) plus (1.28). The parameters of the

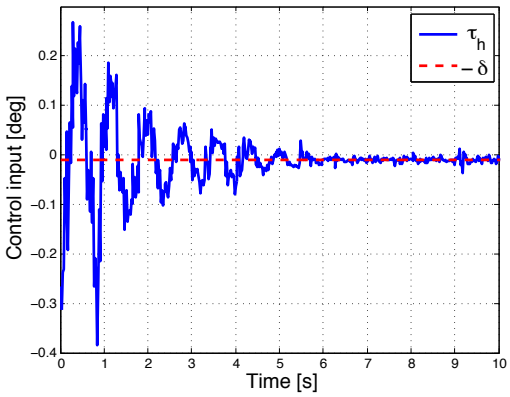

Fig. 1.18 Time history of the control input torque and its value at steady state with the IDA-PBC plus NLPID1 controller.

controller are as follows: $N_{11} = 0.41$, $N_{12} = -0.03$, $N_{22} = 0.003$, $k_2 = 0.00025$, $K_1 = 0.012$, $K_2 = \left(G^\top M_d^{-1} G\right)^{-1}$, $K_3 = 0.06$, $K_v = 0.3$, $\alpha = 0$, $\beta = 0$ and $K_I = 2.2$.

The time history of the most significant variables obtained in this experiment are shown in Figures 1.24 to 1.27. As can be seen in Figures 1.24 and 1.25, the controller is able to balance Disk 2 at the upright position while stabilizing the angle of Disk 1 at the desired set-point. The controller state and the control torque are shown in Figures 1.26 and 1.27, respectively. These plots evidence that the controller ensures internal stability, output regulation and disturbance rejection showing very good performance.

1.4.6 Tracking angle ramp references for the Disk 1.

Finally, we present simulations to assess the performance of the IDA-PBC controller plus the NLPID2 when the reference for the angle of the Disk 1 is a ramp. The ramp reference is $\theta^\star(t) = \alpha t + \beta$, where the constants α and β are chosen to change the shape of the ramp. The controller parameters are as follows: $N_{11} = 0.41$, $N_{12} = -0.03$, $N_{22} = 0.003$, $k_2 = 0.25$, $K_1 = 0.012$, $K_2 = \left(G^\top M_d^{-1} G\right)^{-1}$, $K_3 = 0.2$, $K_v = 0.5$ and $K_I = 3$. The disturbance is set at $\delta = 0.25$ Nm. To increase the realism of the simulations, we have include in the feedback loop a zero-order hold (75Hz), a time delay and noise in the measurements. We also modify the model parameters up to a 10% of their nominal values to emulate uncertainties.

The simulation results are shown in Figures 1.19-1.23. The ramp references and the time history of the Disk 1 angle are depicted in Figure 1.19. This figure shows that the Disk 1 tracks the desired ramp profile, while Figure 1.20 shows that the Disk 2 is kept balanced at the upright position. Figure 1.21 shows that the tracking error of the Disk 1 angle converges to zero as expected. As can be seen in Figure 1.22 the angular velocity of the Disk 1 reaches constant values when the ramp is active, and converge to zero when the reference of the Disk 1 angle is constant. The same

figure shows that the angular velocity related to the balancing angle converges to zero. Finally, Figure 1.23 shows that the control input is sufficiently smooth and bounded between reasonable values.

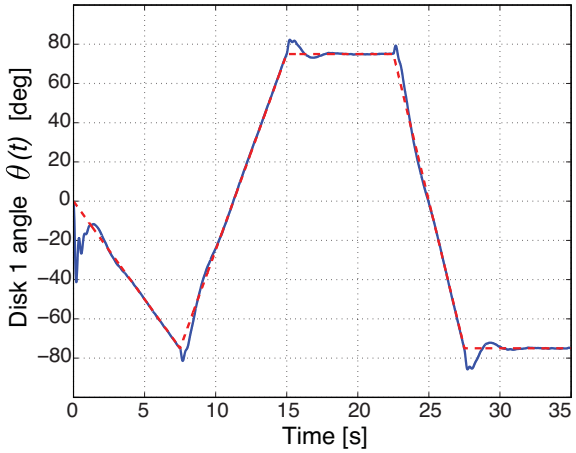

Fig. 1.19 Time history of the Disk 1 angle with ramp references.

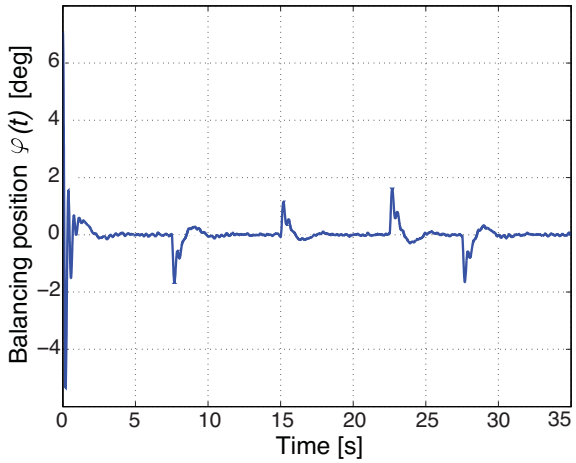

Fig. 1.20 Time history of the balancing angle.

1.4.7 Discussion

As shown in the experiments, the IDA-PBC controller presented in Section 1.3.2 is robust against parameter uncertainties. The action of disturbance, however, deteriorate the performance of the control system. Indeed, the experiments in Section

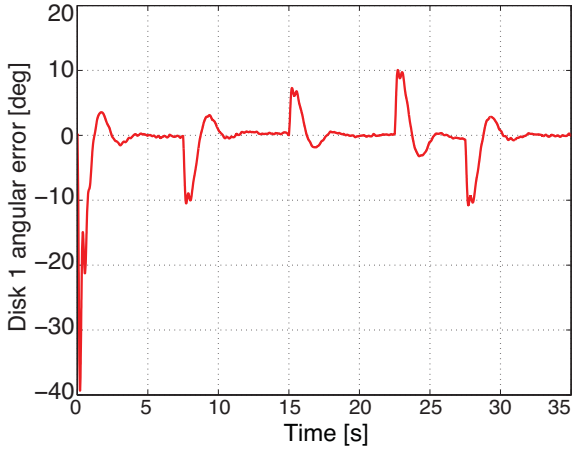

Fig. 1.21 Time history of the error on the Disk 1 angel with ramp references.

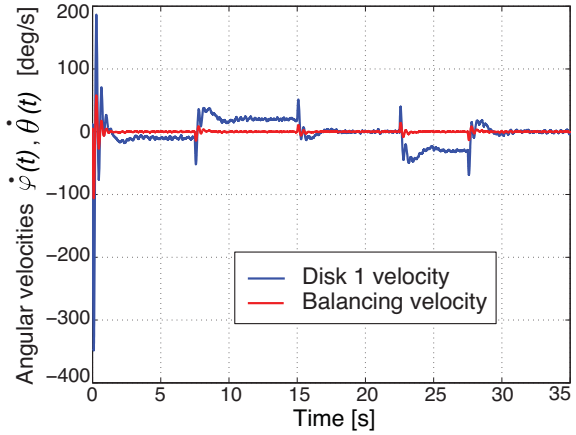

Fig. 1.22 Time history of the angular velocities.

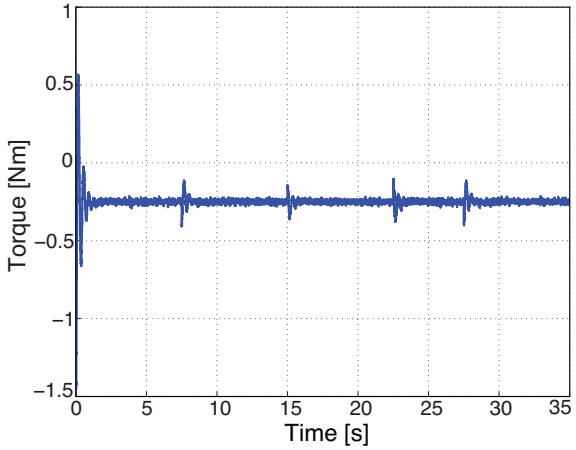

Fig. 1.23 Time history of the control input torque.

1.4.1 show that the IDA-PBC controller balances Disk 2, but the steady-state error of Disk 1 angle is notably large. The classical solution of adding integral action on the passive output does not improve the performance of the controller respect to the standard IDA-PBC as shown in Section 1.4.2. This fact was previously reported in [14], however, no experiment has illustrated this theoretical results before.

The experiments in Sections 1.4.3-1.4.5 show that controllers presented in Section 1.3.4 are able to balance Disk 2 and simultaneously stabilize the angle of Disk 1, thanks to the action of the outer NLPID. However, from the time histories of the states we can see that the rate of convergency of the DoD variables using the controller NLPI is faster that the NLPID1, and produces less oscillations. This better transient performance is, however, darken by the steady state error, which is not present in the NLPID1. Also, the overshoot of Disk 1 angle is greater when using NLPI compared with the NLPID1 at expense of a more demanding control torque. On the other side, the last experiment shows that the controller NLPID2 performs better than the controller NLPI and NLPID1. Indeed, the transient performance of the NLPID2 is better that the other controllers with less overshoot in both the balancing angle φ related to Disk 2 and the angle θ of Disk 1. These angles reach their desired values with less oscillations and with a faster rate of convergency. In addition, the control torque demanded by the controller NLPID2 looks less demanding and smoother than that of the controllers NLPI and NLPID1. As one may expect, all these benefits are at expenses of a more complex controller.

The simulations presented in Section 1.4.6 show that the controller NLPID2 can also track an angle ramp reference for the Disk 1 while keeping the Disk 2 at the balancing position. The integral action of the controller reject the action of constant matched disturbance while ensuring stability. The simulations shown that the control system can follow a continuos profile of the ramps and constant references for the actuated Disk without losing balancing of the non-actuated Disk.

The experiments of the disk-on-disk prototype described in Sections 1.4.3, 1.4.4 and 1.4.5 are summarize in a multimedia video that can be watched on `https://youtu.be/B0k8JtYZjrY`.

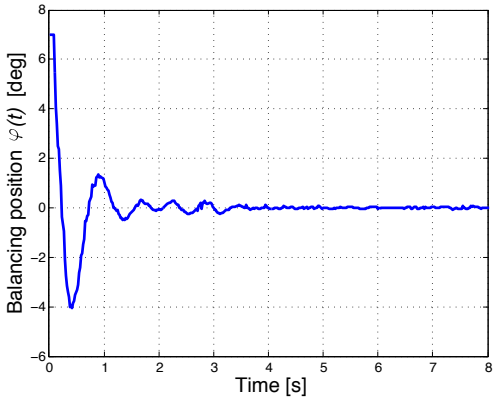

Fig. 1.24 Time history of the balancing angle with the IDA-PBC plus NLPID2 controller.

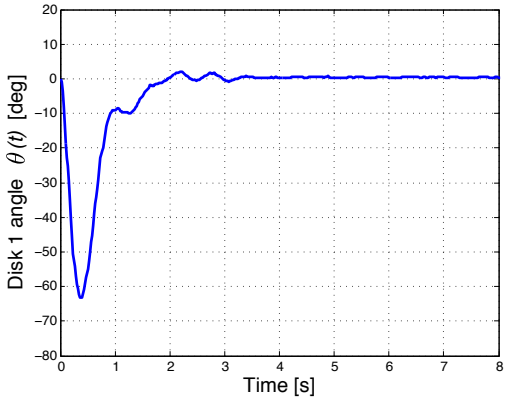

Fig. 1.25 Time history of Disk 1 angle with the IDA-PBC plus NLPID2 controller.

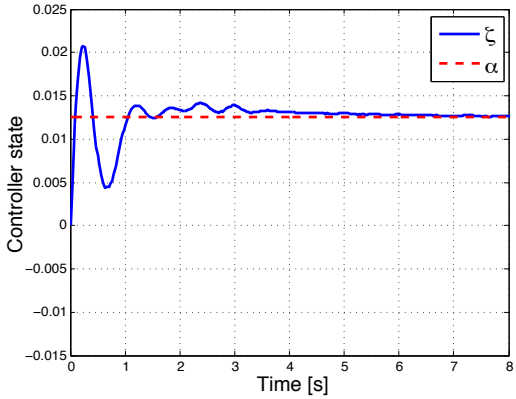

Fig. 1.26 Time history of the controller state and its value at steady state with the IDA-PBC plus NLPID2 controller.

1.5 CONCLUSION

In this chapter we present an IDA-PBC controllers for the disk-on-disk system that is robust to constant matched disturbances. This controller is able to track ramp references for the angle of the actuated disk while keeping the balance of the non-actuated disk. The stabilization of constant angles for the actuated disk can be considered as a reticular case of the ramp reference. We also show simulations and experimental results to evaluate the performance of the control system and evaluate the applicability of nonlinear control techniques based on passivity in a real setup. The robust IDA-PBC proposed in this work exhibit very good performance in both simulations and experiments, which validate the use of this technique on a practical

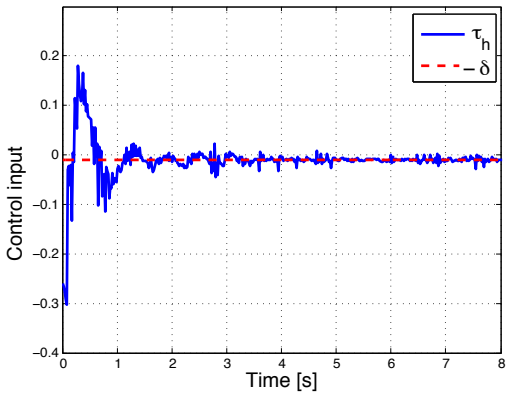

Fig. 1.27 Time history of the control input torque and its value at steady state with the IDA-PBC plus NLPID2 controller.

application. Future research will aim to design controllers for more complex robotic systems performing more involved tasks.

ACKNOWLEDGEMENTS

This work was partially supported by the RoDyMan project, which has received funding from the European Research Council FP7 Ideas under Advanced Grant agreement number 320992. The authors are solely responsible for the content of this manuscript.

The second author acknowledges the National University of Rosario, Argentina, for supporting his internship at PRISMA Lab.

References

[1] M. Crespo, A. Donaire, F. Ruggiero, V. Lippiello, and B. Siciliano. Design, implementation and experiments of a robust passivity-based controller for a rolling-balancing system. In *International Conference on Informatics in Control, Automation and Robotics*, Lisbon, Portugal, 2016.

[2] A. Donaire and S. Junco. On the addition of integral action to port-controlled Hamiltonian systems. *Automatica*, 45:1910–1916, 2009.

[3] A. Donaire, J. G. Romero, R. Ortega, B. Siciliano, and M. Crespo. Robust IDA-PBC for underactuated mechanical systems subject to matched disturbances. *International Journal of Robust and Nonlinear Control (in press)*, 2016.

[4] A. Donaire, F. Ruggiero, L. R. Buonocore, V. Lippiello, and B. Siciliano. Passivity-based control for a rolling-balancing system: The nonprehensile

disk-on-disk. *IEEE Transactions on Control System Technology (accepted)*, 2016.

[5] W. Haddad and V. Chellaboina. *Nonlinear Dynamical Systems and Control. A Lyapunov-Based Approach*. Princeton University Press, New Jersey, 2007.

[6] H.K. Khalil. *Nonlinear Systems*. Prentice Hall, 2002.

[7] C. Lanczos. The variational principles of mechanics. *University of Toronto Press*, 1960.

[8] V. Lippiello, F. Ruggiero, and B. Siciliano. The effects of shapes in input-state linearization for stabilization of nonprehensile planar rolling dynamic manipulation. *IEEE Robotics and Automation Letters*, 1(1):492–499, 2016.

[9] D. Merkin. *Introduction to the Theory of Stability*. Springer Verlag, New York, 1997.

[10] R. Ortega and J. G. Romero. Robust integral control of port-Hamiltonian systems: The case of non-passive outputs with unmatched disturbances. *Systems & Control Letters*, 61(1):11–17, 2012.

[11] R. Ortega, A. Loría, P.J. Nicklasson, and H. Sira-Ramírez. *Passivity-based Control of Euler-Lagrange Systems: Mechanical, Electrical, and Electromechanical Applications*. Springer Verlag, London, 1998.

[12] R. Ortega, M.W. Spong, F. Gomez-Estern, and G. Blankenstein. Stabilization of a class of underactuated mechanical systems via interconnection and damping assignment. *IEEE Transactions on Automatic Control*, 47(8):1218–1233, 2002.

[13] R. Ortega, A. Donaire, and J. G. Romero. *Passivity–based control of mechanical systems*. Lecture Notes in Control and Information Sciences. Springer, Berlin/Heidelberg, 2016.

[14] J. G. Romero, A. Donaire, and R. Ortega. Robust energy shaping contorl of mechanical systems. *Systems & Control Letters*, 62(9):770–780, 2013.

[15] J. G. Romero, R. Ortega, and A. Donaire. Energy shaping of mechanical systems via PID control and extension to constant speed tracking. *IEEE Transactions on Automatic Control*, 61(11):3551–3556, 2016.

[16] J. C. Ryu, F. Ruggiero, and K.M. Lynch. Control of nonprehensile rolling manipulation: Balancing a disk on a disk. *IEEE Transactions on Robotics*, 29 (5):1152–1161, 2013.

[17] B. Siciliano, L. Sciavicco, L. Villani, and G. Oriolo. *Robotics. Modelling, Planning and Control*. Springer Verlag, London, 2009.

[18] M. Spong, S. Hutchinson, and M. Vidyasagar. *Robot Modeling and Control*. John Wiley & Sons, USA, 2006.

[19] A. J. van der Schaft. *L2-gain and Passivity Techniques in Nonlinear Control*. Springer Verlag, 2000.